Applied Catalysis B: Environmental 160–161 (2014) 10–21

Contents lists available at ScienceDirect

Applied Catalysis B: Environmental

journal homepage: www.elsevier.com/locate/apcatb

Hydrotreating activity of bulk NiB alloy in model reaction of hydrodesulfurization 4,6-dimethyldibenzothiophene

M. Lewandowski*

Centre of Polymer and Carbon Materials, Marii Curie Skłodowskiej 34, 41-819 Zabrze, Poland

ARTICLE INFO

Article history:
Received 20 February 2014
Received in revised form 26 April 2014
Accepted 3 May 2014
Available online 10 May 2014

Keywords:
Bulk NiB alloy catalyst
Nickel sulfide (Ni_3S_2)
Hydrogenation
Hydrodesulfurization (HDS)
4,6-Dimethyldibenzothiophene (4,6-DMDBT)
Metallic Ni^0, Ni_3B phase

ABSTRACT

For the first time hydrodesulfurization reaction of 4,6-dimethyldibenzothiophene (4,6-DMDBT) was performed on bulk NiB alloy in the presence of nitrogen compound – carbazole. Before and after reaction the catalysts were characterized by X-ray diffraction (XRD), also by high-resolution transmission electron microscopy (HRTEM), scanning electron microscopy (SEM) and differential scanning calorimetric analysis (DSC) and by X-ray photoelectron spectroscopy (XPS) – after HDS reaction. The surface and metallic phase were determined by N_2 physisorption and CO chemisorption. During the HDS reaction partially formed Ni_3S_2, metallic Ni and Ni_3B were observed. The activity of the catalyst was mainly attributed to the presence of Ni and Ni_3B phases. In the absent of N-compound the main product was the 3-(3′-methylcyclohexyl)-toluene (MCHT) – formed via hydrogenation route (HYD route). At lower contribution of direct desulfurization route (DDS route), products like 3,3′-dimethylbiphenyl (3,3′-DMBPh) were also formed, but no fully hydrogenated product (3,3′-dimethylbicyclohexyl) was observed. In the presence of carbazole the distribution of HDS products was the same, but the activity was lower due to the HDN competition reaction. Based on these results and after calculated kinetics, it can be assumed that the rate of HDS of the 4,6-DMDBT, catalyzed by NiB alloy, is a first order reaction with respect to the substrate concentration for alone process of HDS, while for the same catalyst in case of simultaneous HDS/HDN reactions, this rate is independent of the 4,6-DMDBT concentration (zero-order) in the range of contact times studied.

1. Introduction

In recent years, transition metal borides have become attractive catalytic materials as amorphous alloys – mainly NiB and CoB. Mainly these catalysts were investigated for the hydrogenation reactions. For instance, the examined reaction included borides in the benzene to cyclohexane hydrogenation [1–3], or selective hydrogenation of cyclopentadiene to cyclopentene [4–6]. Besides, the transition metal borides were used in citral to citronellol hydrogenation [7,8], as well as in nitro-compounds reduction [9,10]. However, their applications are not limited to the aforementioned examples.

The particularly interesting feature of borides (NiB and CoB), especially when compared to the classical hydrogenation catalysts [6,11–13], is their sulfur resistance. The available literature provides only few publications concerning these types of materials as hydrotreating catalysts. The two prominent ones were published by Skarabalak and Suslick [14], and by Bussell et al. [15].

Skrabalak and Suslick [14] stated that the NiB and CoB borides are unstable and undergo sulfurization in the first stage of hydrotreating. In turn, Bussell et al. [15] claimed that the catalysts concocted by sulfiding NiB/SiO_2 and $NiMoO\text{-}B/SiO_2$ presented higher activity in the HDS reaction of thiophene than the conventional sulfided catalysts such as Ni/SiO_2 and $NiMo/SiO_2$.

Since 2009 the admissible level of sulfur in diesel oil has been below 10 ppm [16,17]. It may happen in the future that the level of admissible sulfur will decrease to 1 ppm or below, especially for fuel cell applications [18,19]. The sulfur compounds, mainly dibenzothiophene derivatives [20] present in the product, obtained after the first stage of hydrotreating, and the nitrogen compounds such as carbazole and its alkyl derivatives, are highly chemically resistant. Their resistance is related to the steric hindrance because of the alkyl groups [20–22]. The amounts of sulfur and nitrogen compounds left after the first stage of hydrotreating, expressed as S and N content, are 250–300 ppm and nearly 100 ppm respectively [23].

Therefore, the researchers are seeking for new catalytic materials to become potential catalysts or promoters of the second-stage

* Corresponding author at: SYNTHOS S.A. Chemików 1, 32-600 Oświęcim, Building E-182, Poland.
E-mail address: marco297@wp.eu

http://dx.doi.org/10.1016/j.apcatb.2014.05.002
0926-3373/

of hydrotreating. In the case of the nonsulfided materials (examined as the catalysts of second stage of hydrotreating), classical sulfidation as a process for activating a catalyst cannot be applied. What is more, sulfur concentration in the raw material (partial pressure of H_2S in gas) is relatively low, when compared to the partial pressure of H_2S in the classical HDS process based on the NiMo or CoMo catalysts. The possible "sulfidation" of the material may appear only *in situ* during the HDS process and, in such conditions; it does not have to be complete.

Taking into account the above factors: sulfur resistance of transition metal borides (role of boron) and their high hydrogenating activity, which is necessary in the process of the second stage hydrotreating, the research on their activity and the actual resistance in model reaction HDS 4,6-DMDBT has been carried out.

2. Experimental

2.1. Preparation of NiB alloy

The NiB amorphous alloy catalysts were prepared by the chemical reduction method. The solution of KBH_4 (2.0 mol/L) was used as the reducing agent. This solution was added drop-wisely to the solution of nickel salt ($NiCl_2$-0.1 mol/L) in room temperature and under N_2 atmosphere. The mixture was vigorously stirred. The resulting NiB alloy catalyst was washed with distilled water until its pH value was about 7 and then kept in absolute ethanol for future use.

2.2. Characterization

The materials were characterized by XRD, TEM, SEM, DSC, XPS, BET measurements and CO chemisorptions. Additionally, elemental chemical analysis of nickel, boron and carbon, hydrogen, nitrogen and sulfur (CHNS) after HDS/HDN reaction was performed.

2.2.1. X-ray diffraction

Structural characterization of NiB catalyst before and after reactions was carried out by X-ray diffraction (XRD) using a SIEMENS D-500 automatic diffractometer with the CuK_α monochromatized radiation. The amount of amorphous phase and crystallinity of the boride obtained were estimated from the intensity of all reflections in the range 2θ from 10° to 90°.

2.2.2. TEM, SEM and DSC analysis

TEM: High-resolution transmission electron microscopy (HRTEM) analysis was carried out on fresh and heated NiB alloy. The HRTEM study was performed using a JEOL 200 CX electron microscope.

SEM: scanning electron microscopy (SEM) was performed for NiB catalysts after HDS/HDN reactions. The SEM study was performed using a FEI electron microscope model Quanta FEG250.

DSC: Differential scanning calorimetry (DSC). Calorimetric measurements were carried out using a differential scanning calorimeter (TA Instruments DSC 2920) in a dry nitrogen atmosphere (50 ml/min). Calibration was carried out with a high purity indium. For all DSC experiments, small quantities of the sample, about 7 mg, were crimped into standard nonhermetical aluminum pans. Samples were quenched using liquid nitrogen to about 20 °C and then reheated to 550 °C at 10 °C/min. The obtained results were collected and analyzed using Universal Analysis NT Software.

2.2.3. XPS analysis

X-ray photoelectron spectroscopy (XPS) was performed on a Kratos AXIS165 spectrometer with X-Ray Gun: mono Al Kα radiation ($h\nu$ = 1486.58 eV). For calibration the C 1s line at 284.8 eV was used as charge reference. Server and narrow regions of spectra were acquired at pass energies of 160 eV and 20 eV respectively. Error in estimating bond energies was ±0.1 eV.

2.2.4. Specific surface area (SSA) measurements

Specific surface area (SSA) was measured for the fresh samples and after catalytic reactions. The specific surface area of the samples was determined from the N_2 adsorption isotherms at 77 K on an ASAP2010 apparatus (Micromeritics).

2.2.5. Dynamic CO titration – pulsed technique

CO uptake is a classical technique used to titrate the metallic sites. The CO uptake was performed "*in situ*" i.e., in the synthesis reactor without exposing the fresh NiB alloy to air or to the passivating mixture. Known quantity of CO (17 μmol) was injected, at regular intervals, to the sample conditioned at RT in flowing He (40 mL min^{-1}), purified by an oxygen trap (Oxysorb, messer Griesheim). After each injection, the quantity of probe molecules, which were not chemisorbed, was measured using a conventional device equipped with a TCD. The injections were continued until CO saturated the surface. Data were processed and the number of micromoles of CO chemisorbed per gram of sample was determined.

2.2.6. Elemental chemical analysis

2.2.6.1. Nickel and boron. Elemental analysis for nickel and boron composition has been conducted with the ICP method with the ULTIMA 2 spectrometer. The sample was mineralized with the Multiwave 3000 mineralizer.

2.2.6.2. Carbon, hydrogen, nitrogen and sulfur. Elemental analysis of NiB alloy after HDS alone and after the simultaneous HDS/HDN reactions were performed with FlashEA 2000 Thermo Scientific CHNS analyzer. The sample as weighed in tin capsules, placed inside the MAS 200R autosampler at a preset time, and then dropped into an oxidation/reduction reactor, kept at a temperature of 900–1000 °C. The exact amount of oxygen required for optimum combustion of the sample was delivered into the combustion reactor at a precise time. The reaction of oxygen with the tin capsule at elevated temperatures generates an exothermic reaction which raises the temperature to 1800 °C for a few seconds. At this high temperature both organic and inorganic substances are converted into elemental gases (CO_2, H_2O, SO_2, NO_x) which, after further reduction (NO_x to N_2), are separated in a chromatographic column and finally detected by a highly sensitive thermal conductivity detector (TCD).

2.3. Catalytic tests – hydrodesulfurization

The simultaneous HDS/HDN and alone HDS reactions were carried out with a down-flow fixed-bed microreactor in a high-pressure flow system. The catalyst (0.8 g) was mixed with carborundum at the ratio = 1/5 catalyst to SiC. The liquid feed was fed to the reactor by a high-pressure piston pump through heated stainless tubes. The hydrogen flow (60–360 cm^3 min^{-1}) and total pressure were controlled by a mass flow controller and a back-pressure regulator, respectively. The temperature of the oven was regulated using a temperature controller.

The contact time (t_c) was defined as follows: t_c (s) = catalyst volume (cm^3)/(H_2 flow + feed flow) (cm^3 s^{-1}). The range of applied contact time ranged from 0.37 to 2.19 s.

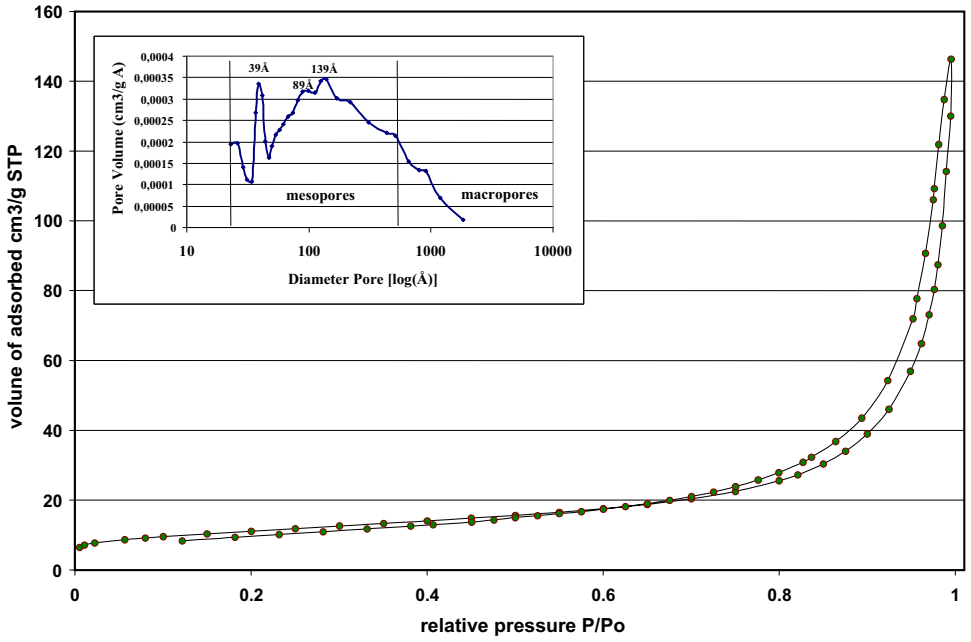

Fig. 1. Adsorption–desorption of nitrogen curves with pore-size distribution (BJH method in left corner) for NiB alloy.

The conversion (conv.) of 4,6-DMDBT and degree of HDS of 4,6-DMDBT were defined following:

$$\text{conv. of 4, 6-DMDBT [\%]} = \frac{S_S}{S_S + S_{4,6\text{-DMDBT}}} \times 100$$

$$\text{degree of HDS [\%]} = \frac{S_H}{S_S + S_{4,6\text{-DMDBT}}} \times 100$$

where S_s is the sum of molar % of all products formed after catalytic transformation of 4,6-DMDBT (including sulfur containing compounds). $S_{4,6\text{-DMDBT}}$ is the molar % of 4,6-DMDBT still present after reaction. S_H is the sum of molar % of all non sulfur containing products formed after catalytic transformation of 4,6-DMDBT.

The liquid products of the reaction were collected every hour in the condenser, which temperature was maintained at 15 °C. Finally, this liquid was analyzed by gas chromatography (HP 4890) using a capillary column (HP1, 30 m × 0.25 mm × 0.25 μm) and a FID detector. The product identification was confirmed by GC/MS analysis with capillary column DB5, (30 m × 0.25 mm × 0.25 μm).

The HDS reaction of 4,6-dimethyldibenzothiophene was performed simultaneously and separate at 350 °C, under a total pressure of 6.0 MPa with a molar H_2/feed ratio of 600. The liquid feed contained 0.17% 4,6-DMDBT (300 ppm S) and/or 0.08% carbazole (100 ppm N for competition reaction) in o-xylene. Before starting the catalytic tests, each catalyst was reduced in situ at 623 K (350 °C) for 2 h in pure dihydrogen atmosphere. The catalytic process was conducted for about 100 h. After about 100 h, the initial operating conditions were reset in order to check again the activity of the catalyst. The conversion of solvent was checked over all catalyst. It was observed that practically no conversion of the solvent took place in the operating conditions.

3. Results

3.1.1. CO chemisorption

The experimental CO uptakes of the sample of bulk NiB alloy (after heating at 350 °C for 6 h in presence of H_2 atmosphere in situ) was 109.3 μmol g^{-1}. The stoichiometry factor for CO chemisorptions on Ni metal is 2 (1 CO molecule for 2 atoms of Ni – bridge type CO molecularity adsorption). Therefore, as calculated there is 54.7 μmol of Ni atoms per gram on the surface of the bulk NiB alloy, which is equal to 8.48×10^{17} atoms of Ni per 1 m^2 of catalyst surface. On the basis of the chemisorptions of CO, it was found that the surface area of nickel atoms constitutes about 5.5% of the total specific surface area of the catalyst.

3.1.2. Textural properties

The specific surface area of the NiB alloy catalysts was found to be 38.8 m^2/g.

The nitrogen adsorption–desorption isotherm of the bulk NiB alloy is shown in Fig. 1. According to Brunauer [24], the shape of the isotherm of nitrogen adsorption indicates that it can be classified as type IV. On the other hand, the presented adsorption–desorption hysteresis loop of bulk NiB alloy catalyst may be classified as H1 according to the IUPAC classification [25,26] (formally type A according to De Boer's [27,28]). This type of hysteresis is characteristic for solids consisting of particles crossed by nearly cylindrical channels or solids made by aggregates or agglomerates of spheroidal particles [26].

The hysteresis loop of the bulk NiB alloy catalyst leads to the conclusion that the type A may be assigned to the presence of tubular (cylindrical channels) capillaries with different shapes, opened at both ends, or to the formation of a porous network. The relatively high value of $p/p_o = 0.7$ indicates a significant number of larger pores (mesopores). The pore size distribution for NiB alloy is also illustrated in Fig. 1 (in left corner). Most of the pore volume relates to mesopores (20–500 Å) with a three local maximum for pores diameters of 39, 89 and 139 Å respectively. Generally, NiB alloy consists mainly of mesopores and relatively small amount of macropores (>500 Å).

After the catalytic test was performed, the specific surface areas decreased to 10.9 m^2/g (alone HDS) and 10.5 m^2/g (after simultaneous HDS/HDN reaction) respectively. The main reason of this decrease is due to crystallization of samples during the reaction (temperature of reaction) and partially due to sulfidation during the alone and simultaneous HDS/HDN reactions.

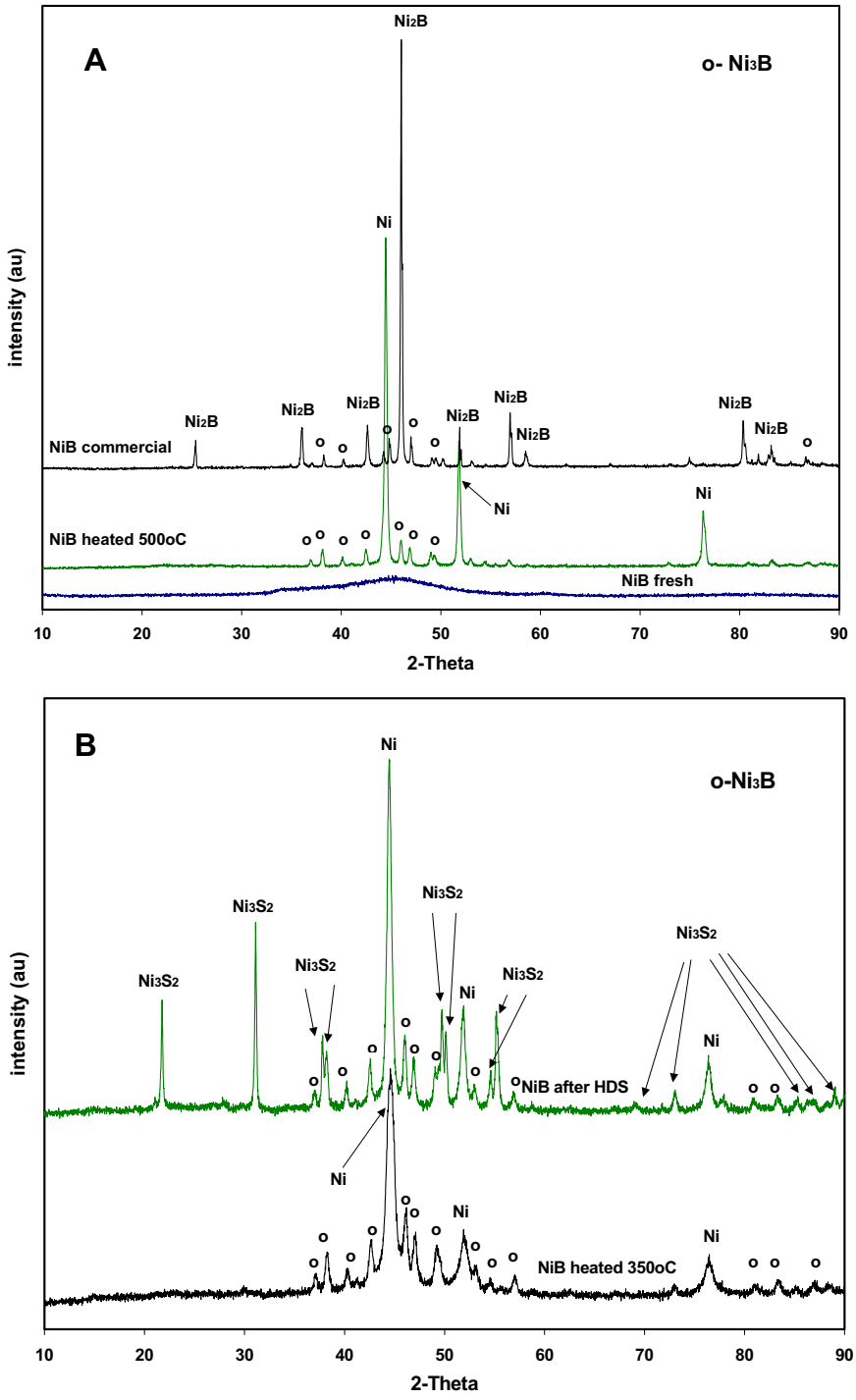

Fig. 2. X-ray diffraction patterns (A) fresh bulk NiB alloy, heated at 500 °C and commercial NiB, (B) NiB alloy heated at 350 °C and after HDS.

3.1.3. XRD diffraction

Fig. 2A shows the diffraction patterns of the bulk NiB alloy catalyst (fresh) and after being heated at 500 °C and comparison of these patterns with commercial NiB.

The XRD pattern of the NiB catalyst after the fresh synthesis (Fig. 2A) presents only the wide peak for $2\theta = 45°$ typical for the amorphous structure of NiB alloy [29]. In turn, the XRD pattern of the sample heated for 6 h at 500 °C in the hydrogen flow (Fig. 2A) presents three clear peaks coming from metallic Ni (JCPDS #01-071-3740). The remaining, relatively small peaks visible on the sample pattern are related to the Ni_3B phase (JCPDS #01-082-1699). This shows substantial decomposition of an alloy into metallic Ni and elemental boron during heating. The elemental boron peaks are not visible on the XRD pattern, because of the low concentration of boron and its high dispersion [30,31]. The XRD pattern of the commercial NiB presents peaks (Fig. 2A) typical for the Ni_2B phase (JCPDS #00-048-1222). The other small peaks are connected with the Ni_3B phase (JCPDS #01-073-1792). Thus, it may be claimed that the commercial NiB consists mostly of the Ni_2B phase, as stated by a producer.

Fig. 2B shows the pattern of the NiB catalyst after the HDS process, together with the spectrum of the NiB sample subjected only to 8-hour heating in hydrogen flow at the reaction temperature of

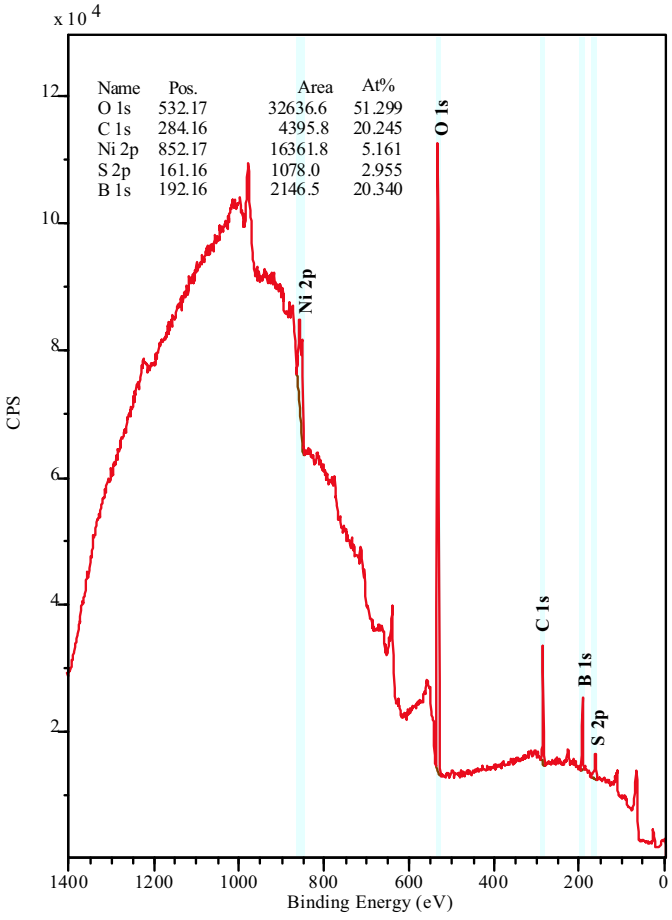

Fig. 3. Survey XPS spectra of NiB catalysts after HDS/HDS reaction.

350 °C. The pattern of the hydrogen-heated sample shows three relatively big peaks, all typical for the metallic Ni (JCPDS #01-071-3740). The remaining peaks visible in this pattern are related to the presence of the crystallographic Ni_3B phase (JCPDS #01-073-1792). This proves that crystallization process and partial decomposition of the alloy took place after heating [32].

The pattern of the catalyst sample after the HDS process resembles the pattern of the sample subject only to heating. However, there are new relatively big peaks visible, mainly for $2\theta = 21.75°$ and 31.10°, and several smaller ones (Fig. 2B) typical for crystallographic phase of Ni_3S_2 (JCPDS #00-030-0863), specific for the low-temperature structure of the Ni_3S_2 sulfide of the heazlewoodite-phase type [33]. The remaining peaks visible on this sample (Fig. 2B) may be related to the presence of either metallic Ni (JCPDS #01-071-3740) or the Ni_3B phase (JCPDS #01-073-1792). This proves that both crystallization and partial decomposition of the alloy are related to the reaction temperature and that catalyst sulfidation has taken place in these conditions. Presence of the Ni and Ni_3B phases shows that the sulfidation process, which took place during the reaction, is not complete.

3.1.4. X-ray photoelectron spectroscopy (XPS)

Fig. 3 shows XPS spectra of the studied catalyst including Ni $2p_{3/2}$, O 1s, B 1s and S 2p lines together with quantification from survey spectra (atomic %) of the surface of the catalyst. Fig. 4 shows the Ni $2p_{3/2}$ XPS spectra with four peaks at binding energies of 852.6 eV, 853.9 eV, 856.7 eV and 861.8 eV respectively after deconvolution. The first peak (852.6 eV) in Ni $2p_{3/2}$ level is assigned to metallic nickel (Ni^0) [34–36]. The second main peak

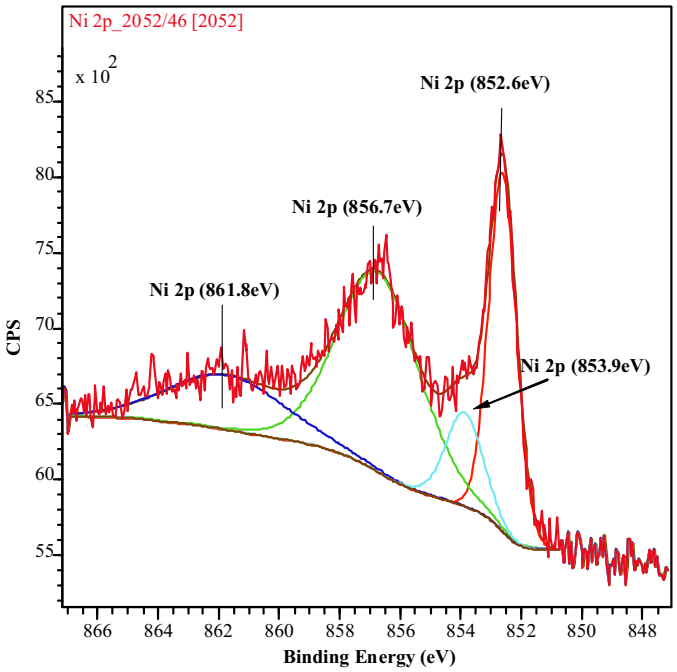

Fig. 4. Ni $2p_{2/3}$ XPS spectra of surface of NiB catalyst after HDS/HDN reaction.

(856.7 eV-satellite peak) is attributed to the presence of oxidized nickel (NiO) [34]. The remaining peak (853.9 eV) in Ni $2p_{3/2}$ level is assigned to the Ni, which is present in the NiB alloy. The Ni $2p_{3/2}$ binding energies for the borides are slightly higher than that for Ni^0 [34]. The associated satellite peak near 861.8 eV indicates the presence of more than one "nickel-oxygen" species on the surface of catalyst. The S(2p) spectrum shown in Fig. 5A includes two well resolved peaks of sulfur at 162.3 eV and 163.6 eV corresponding to S $2p_{2/3}$ and S $2p_{1/2}$ respectively and assigned to Ni_3S_2 [37]. In case of B(1s), the spectrum (Fig. 5B) contains only one peak near 193.0 eV, corresponding to oxidized boron- B_2O_3 [34]. This value is far from the value obtained for pure B (186.7 eV). Only one peak is observed, due to surface oxidation during the removal of catalyst from the reactor and separation from SiC resulting from inevitable contact with air before storage in absolute ethanol. It should be noted that oxidized boron is always present in the prepared catalyst, no matter which preparation method was employed [12].

3.1.5. Elemental analysis

The quantitative composition of the prepared catalysts, obtained after elemental analysis, was as follows: 87.2% of nickel and 7.1% of boron, which corresponded to the stoichiometric ratio of Ni to $B = 2.26:1$. In the prepared catalysts, the molar ratio of nickel to boron equaled nearly 2 to 1, which is typical for such systems according to the other authors [15,38]. The elemental analysis of the catalyst after HDS alone and in presence of N-compound (carbazole) are shown in Table 1.

Based on these results, it was calculated, that only about 26.2% of Ni was transformed into Ni_3S_2 during the catalytic tests and level of sulfidation of catalyst was similar in both cases. On the basis of the

Table 1
Elemental analysis of NiB catalyst after HDS alone and simultaneous HDS/HDN reactions.

NiB catalyst	N [ppm]	C [%]	H [%]	S [%]
After HDS	–	0.93	1.03	8.92
After HDS/HDN	713	0.85	0.88	8.33

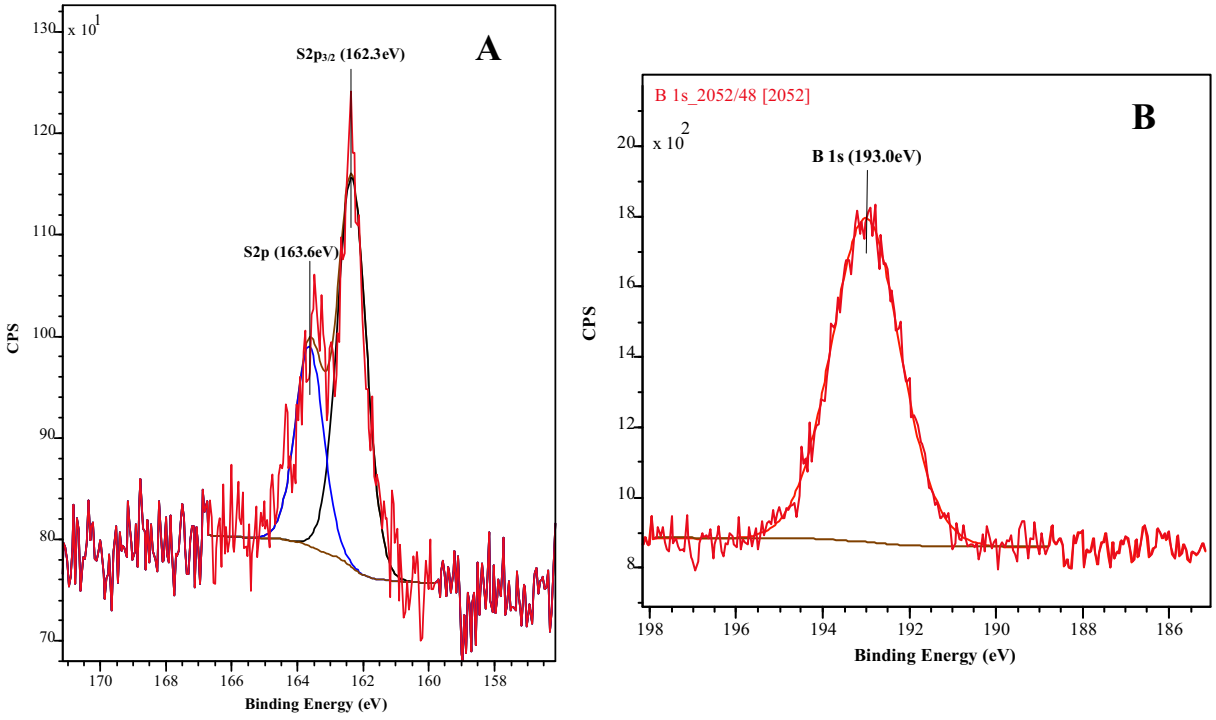

Fig. 5. (A) S 2p and (B) B 1s XPS spectra of surface of NiB catalyst after HDS/HDN reaction.

CO chemisorptions and the elemental analysis it can be concluded, that the surface of NiB alloy is rather poor in Ni surface atoms.

3.1.6. SEM and TEM analysis

The SEM and TEM pictures revealed that the fresh NiB alloy sample can be modeled as small spherical particles organized as a sponge–like regular morphology comprised of small particles, as presented in Figs. 6 and 7A. The NiB alloy particles have the characteristic of nanoparticles, with an average particle site ranging between 15 and 80 nm and being interconnected. The SAED morphology of the bulk NiB alloy sample (shown in upper left of corner in Fig. 7A) is a Debye rings rather than distinct dots in the SAED image of NiB alloy, which was also employed to verify the

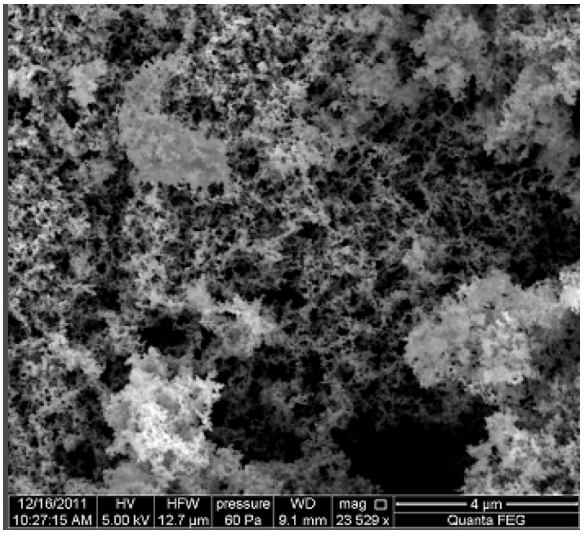

Fig. 6. SEM surface morphology of NiB fresh alloy catalyst.

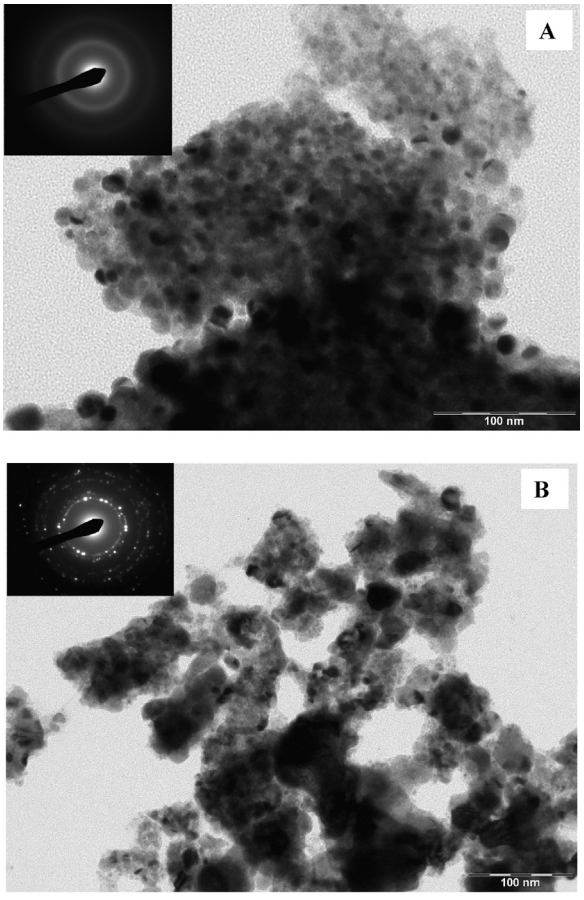

Fig. 7. TEM morphology of NiB alloy (A) fresh catalyst with SAED pattern and (B) catalyst after heating at 350 °C with SAED pattern.

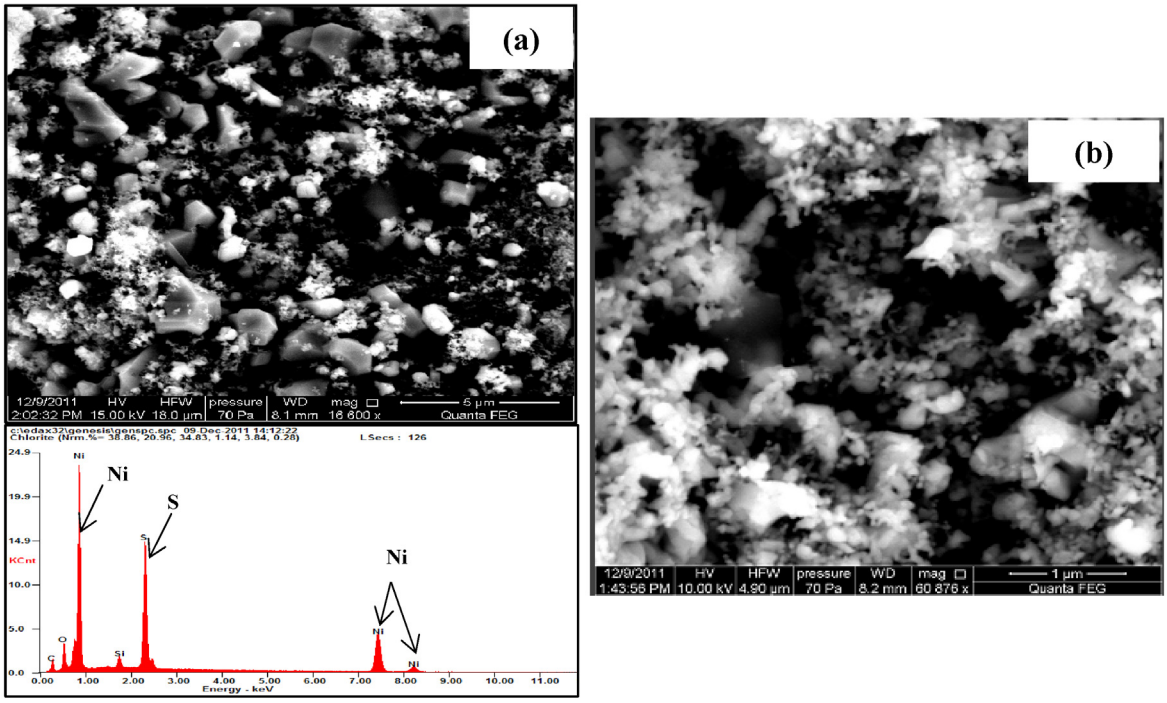

Fig. 8. SEM morphology of NiB alloy catalyst (a) after HDS reaction at 350 °C with EDX analysis and (b) enlargement of selected part of sample.

amorphous structure of NiB catalyst. This is in a good agreement with the XRD results presented in Fig. 2A.

The crystallization of the NiB alloys in 350 °C in H_2 atmosphere is unambiguous. At this temperature coalescence of small particles into bigger one takes place. This is also confirmed by SAED on selected grain domain of NiB alloy, which is presented as an insert in the left corner of Fig. 7B. In this case distinct dots in the SAED image of the sample are present, indicating that a highly ordered crystal is formed.

Fig. 8a presents the SEM pictures with EDX analysis of the NiB catalyst after HDS reaction at 350 °C. The picture shows a mixture of crystalline (mainly) and also partially amorphous morphology. This evidence can be seen in the selected part of domain presented in Fig. 8b. The crystalline parts are the mixture of Ni and Ni_3S_2 crystallites detected by XRD analysis. On the other hand, amorphous parts presented by Ni_3B phase, are also detected by XRD, as presented in Fig. 2B.

The EDX analysis confirms the results of the elemental analysis (Table 1). The dominating peaks relates to the to presence of nickel and sulfur. The presence of the small peaks reflecting silicon is caused by the presence of SiC in the sample after reaction. SiC was used as diluter of catalyst. It was extremely difficult to separated catalyst from SiC very precisely.

3.1.7. DSC analysis

The DSC analysis of the fresh NiB alloy is presented in Fig. 9. First large endothermic peak is related to the of ethanol evaporation from sample, as catalyst was stored in ethanol to prevent oxidation. Two exothermic peaks are observed. The first process, starting at 590 K (317 °C) with maximum temperature at 604 K (331 °C), is the formation of various crystalline phases like Ni_2B and Ni_3B [31]. The second one, starting at 718 K (445 °C) {maximum temperature over 749 K (476 °C)} indicates the decomposition of NiB alloy into metallic nickel and free boron. Most of the Ni_3B crystallites are decomposed [31]. The calculated values of enthalpy were equal to 43.3 and 88.8 J/g respectively. This transformation is agreement with the XRD results, presented earlier in Fig. 2A and B. Additionally, these results are also in good agreement with research carried by Wei et al. [39]. Authors [39] ascribe the formation of the first peak to the formation of nanocrystalline Ni and Ni_3B. At higher temperatures, amorphous NiB alloy can be crystallized, which leads to the formation of metallic nickel.

3.2. Hydrodesulfurization

Fig. 10 shows correlation between conversion and degree of HDS as a function of contact time for the bulk NiB alloy. Fig. 10 presents correlations obtained in the HDS 4,6-DMDBT process conducted alone and simultaneously with the carbazole HDN reaction.

For both reactions HDS 4,6-DMDBT with and without the parallel carbazole HDN reaction the margin between conversion and its degree of HDS equaled about 10% for the contact times $t_c < 1.1$ s. For the longest contact time the margin was much lower – 1 to 2%. Fig. 10 shows clearly that the parallel HDN carbazole process (as a competitive reaction) lowers conversion and the degree of

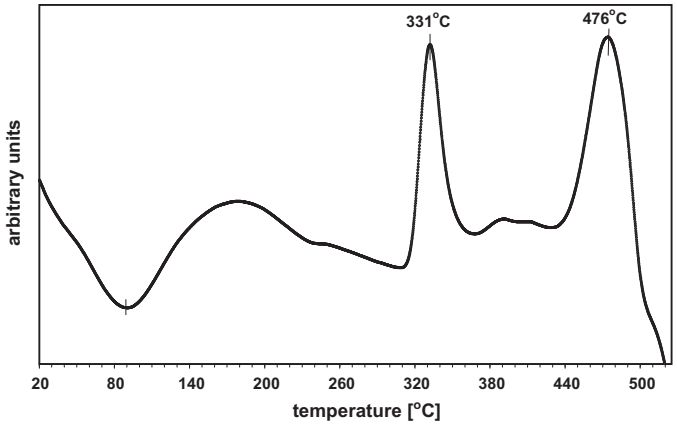

Fig. 9. DSC curve of NiB alloy.

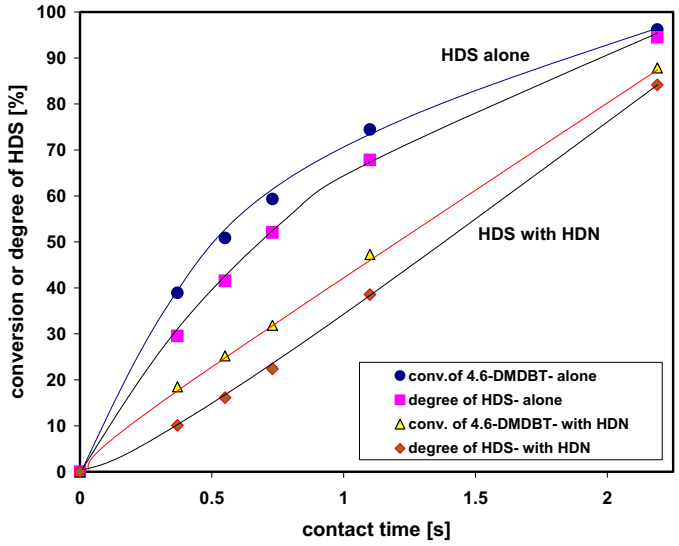

Fig. 10. Conversion and degree of HDS vs. contact time over NiB alloy – HDS reaction alone and together with HDN of carbazole.

HDS by about 20–30% for $t_c < 1.1$ s compared to the HDS process alone. Thus, it may be assumed that the inhibiting effect (competition reaction) of the parallel HDN reaction was substantial for lowering the HDS activity of the catalyst. However, this adverse effect becomes weaker when the HDN reaction achieves 100% of denitrogenation for $t_c = 2.19$ s. Fig. 11A and B shows product distribution of 4,6-dimethyldibenzothiophene (4,6-DMDBT). The results presented in Fig. 11A correspond to the HDS reaction alone, and the ones in Fig. 11B correspond to the HDS reaction with the parallel carbazole HDN reaction.

During the reaction, a process intermediate is formed – 4,6-dimethyltetrahydrodibenzothiophene (4,6-DMTHDBT), which maximum yield of about 8.5% is obtained at $t_c = 0.37$ s in the HDS process alone (Fig. 11A) and at $t_c = 0.55$ s (Fig. 11B) for the parallel HDS/HDN reactions. MCHT was the main product of the reaction. 3,3′-Dimethylbiphenyl (3,3′-DMBPh) was obtained in much lower quantity. Among the products of the reaction, no 3,3′-dimethylbicyclohexyl (3,3′-DMBCH) was found as a product of complete hydrogenation. When the contact time was increased from $t_c = 0.73$ s to $t_c = 2.19$ s, the amount of MCHT more than doubled in both types of reaction, as presented in Fig. 11A and B. However, it may be observed that for the same contact time range (i.e. 0.73–2.19 s) the amounts of 3,3′-DMBPh increased only slightly: from 16% ($t_c = 0.73$ s) to about 20% at the longest contact time, $t_c = 2.19$ s, for the process without carbazole HDN (Fig. 11A). Hence, it may be assumed that for $t_c > 0.73$ s the amount of the obtained 3,3′-DMBPh was hardly dependent on the applied contacts time, whereas in the case of the HDS reaction ran with the parallel HDN reaction (Fig. 11B) the amount of 3,3′-DMBPh was lower and highly dependent on the contact time. For $t_c = 0.73$ s yield of 3,3′-DMBPh was low and equaled about 4% but quadrupled to be 16% for $t_c = 2.19$ s.

High discrepancies in the obtained amounts of MCHT and 3,3′-DMBPh appeared for contact times $t_c < 1.1$ s, when comparing HDS processes with and without the HDN reaction. For MCHT the quantitative margins oscillated between 20 and 30% in favor of the HDS process itself (Fig. 11A). In turn, at the longest contact time $t_c = 2.19$ s the yield margins of both products (3,3′-DMBPh and MCHT) were relatively small when comparing the two variants and equaled, subsequently, 4% for 3,3′-DMBPh and about 8% for MCHT.

Generally, in both cases the reaction runs according to two routes: DDS – direct desulfurization route providing the

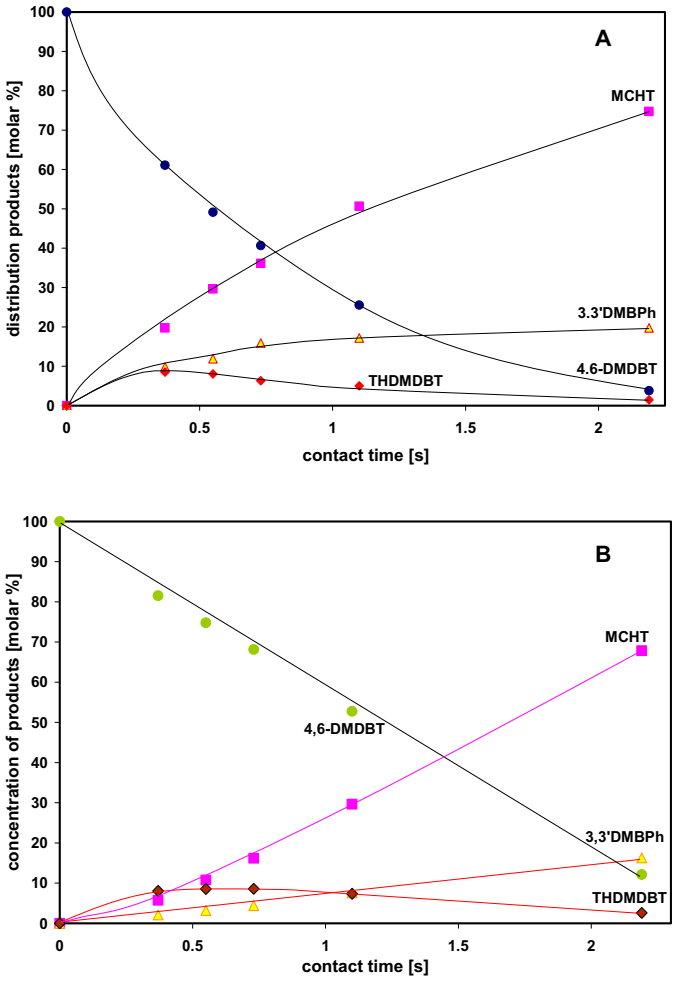

Fig. 11. Products distribution for the HDS of 4,6-DMDBT over NiB alloy (A) alone HDS reaction and (B) HDS reaction together with HDN of carbazole.

3,3′-DMBPh product, and HYD – hydrogenation route producing MCHT. In both cases of hydrodesulfurization, with and without the parallel carbazole HDN reaction, the hydrogenation route was the dominant one, which resulted in the high yield of MCHT.

The commercial bulk alloy NiB was not active for the HDS 4,6-DMDBT reactions in the conditions applied.

3.3. Stabilization of catalysts

The stabilization of NiB alloy for conversions of 4,6-DMDBT in alone and the simultaneous reactions of HDS/HDN versus the time on stream is presented in Fig. 12. The catalytic process was conducted for about 100 h. After this time, the initial conditions of the reaction were reset (initial contact time) and the reaction was continued to obtained stable catalytic activity again (after about additional 10 h). In both cases of HDS reaction of 4,6-DMDBT, little decreased of conversion of 4,6-DMDBT (about 9%), was observed a in applied conditions and ranges of run time. For the longest contact time ($t_c = 2.19$ s) the difference in conversion is relatively small (about 10%) for both reactions (HDS and HDS with HDN). For shorter contact time ($t_c \leq 1.10$ s) the difference is larger and is in the range of 20–28% – due to competition HDN reaction of carbazole. Coke formation is the main reason of a decrease of the 4,6-DMDBT conversion – about 0.9% of carbon was formed on the surface of NiB after HDS reaction. In the case of 20%Ni/SiO_2 catalyst (reference catalysts – results not presented here) decrease of the conversion of about 40% was observed, if compared to about 9% for

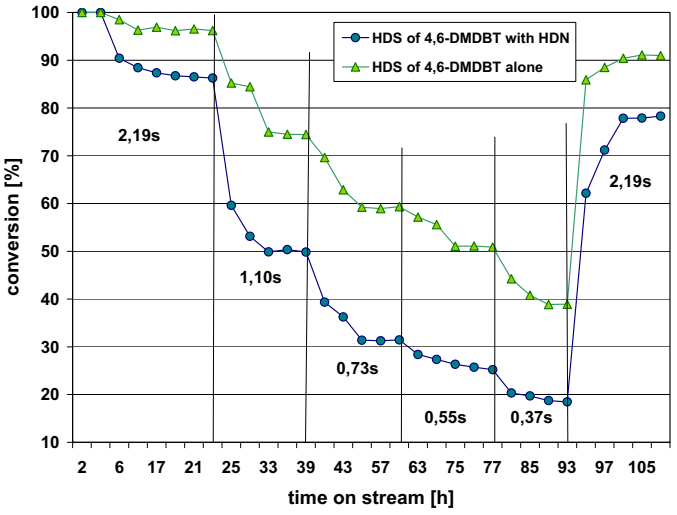

Fig. 12. Stabilization of conversion for NiB alloy catalyst versus time on stream for HDS of 4,6-DMDBT alone and together with HDN of carbazole.

NiB alloy catalyst tested under the same procedure and reaction condition.

4. Discussion

4.1. XRD

The XRD study shows (Fig. 2A) that the wide peak at $2\theta = 45^\circ$ corresponds to the amorphous structure of the NiB alloy [31,40,41], and the temperature increase up to 500 °C causes clear separation of the alloy into metallic Ni and creation of crystallite Ni_3B [42]. The XRD pattern of the commercial NiB alloy (Fig. 2A) complies with the structure of the Ni_2B crystallites, as suggested by the producer.

Besides, the patterns presented in Fig. 2B suggest that the temperature of 350 °C (temperature of HDS/HDN reaction) causes segregation of the alloy into Ni and creation of crystallite blend of Ni_3B/Ni_2B [31]. Although the spectrum of the NiB alloy after the HDS process is quite similar to the pattern of the sample only heated in H_2 at 350 °C, there are new clear peaks assigned to the resultant Ni_3S_2. Therefore, it may be assumed that during the catalytic test a catalyst undergoes partial sulfidation.

However, apart from the sulfide phase, there are still metallic Ni and crystallites Ni_3B (temperature impact) which are responsible for the activity of the catalyst. Thus, in this case the system consists of Ni, Ni_3S_2, Ni_3B, and boron which is not visible on the XRD patterns, due to its relatively low amount and high dispersion [30,31]. The results obtained from XRD studies are in accordance with the XPS surface study, which also indicate presence of metallic nickel. The spectrum S 2p (Fig. 5A) also suggests the partial presence of nickel sulfide. The peak related to the presence of B_2O_3, seen in the spectrum of B 1s (Fig. 5B), is due to inevitable oxidation of the catalyst surface during removal from the reactor after the reaction and separation of SiC.

Skrabalak and Suslick [14] mentioned also thermal instability of the bulk Ni(Co)B during the conditions of deep sulfidation (450 °C and 10%H_2S/H_2). They observed that some part of the boride phase was still present on the catalyst, which was confirmed by our study (presence of Ni_3B). However, this case is not a classical sulfidation of a sample, as during the HDS process the partial pressure of H_2S, produced *in situ* during the HDS reaction, was incomparably lower than during the classical sulfidation procedure. The reaction temperature was also lower (350 °C) than temperature of classical sulfidation – 400 to 450 °C.

Thus, the conditions applied for the HDS process have not led to complete sulfidation of the sample. Similar results have been obtained by Bezverkhyy et al. [43] when studying the interaction between thiophene and Ni/SiO_2. The authors suggested that the interaction between thiophene and the catalyst was not direct. According to their suggestion, first, thiophene (here 4,6-DMDBT) is subjected to the desulfurization reaction and then the resultant H_2S reacts with Ni (NiB). In the applied conditions partial pressure of the resultant H_2S may reach equilibrium values for the Ni/Ni_3S_2 system. When S-compounds act as the source of sulfur, the catalytic reaction brings up two additional factors: (i) change the conversion of S-compounds (change the contact time–the space velocity) and therefore change the partial pressure of H_2S, (ii) on sulfidation the catalytic activity of a metal can provoke the change of H_2S partial pressure. In our case the ratio p_{H_2S}/p_{H_2} was in range from 3.1×10^{-4} to 6.2×10^{-6}. This ratio depends to conversion of DBT (in our case 4,6-DMDBT) and contact time of HDS reaction (flow of feed and H_2). In such case sulfidation is not complete [43]. What's more, as the chemisorption is exothermic reaction, an improved sulfur removal should be expected when increasing the temperature [44]. Also, the chemisorption of H_2S on surface of Ni is reversible, the coverage being a function of the ratio p_{H2S}/p_{H2}. A saturation layer was observed in the temperature 550–645 °C at ratio $p_{H_2S}/p_{H_2} = 2 - 5 \times 10^{-6}$, whereas bulk sulfide ($Ni_3S_2$) was formed at ratio about 10^{-3} according to the thermodynamic data [44,45].

The relative stabilities of sulfides vary with reactions conditions [43,46] – as mentioned above. In the HDS atmosphere involving the presence of H_2 and H_2S in gas phase in chemical equilibrium with the sulfide particles, sulfide particles should be reduced according to the reaction [46]:

$$Ni_3S_2 + xH_2 \leftrightarrow Ni_3S_{2-x} + xH_2S$$

In other site the reduction of bulk Ni_3S_2 into metallic nickel may take place as the lowest limit of sulfur chemical potential according to the chemical equilibrium [46]:

$$Ni_3S_2 + 2H_2 \leftrightarrow Ni + 2H_2S$$

So, Ni_3S_2 is not stable for p_{H_2S}/p_{H_2} ratio is lower than 10^{-5} [46]. As mentioned above for our case the ratio of p_{H_2S}/p_{H_2} was in range from 3.1×10^{-4} to 6.2×10^{-6}. For the temperature of reaction (350 °C) the equilibrium value p_{H_2S}/p_{H_2} is equal 2.51×10^{-5} [47].

It's well known, that among the metals: Ni, Pt and Pd, the affinity of metal to sulfur decreases in order: Ni-S > Pt-S > Pd-S [48]. It means, that Ni is the least resistance for the presence of sulfur (H_2S), because of thermodynamic equilibrium between metal and metal sulfide [48,49]. However, the tolerance for sulfur (the equilibrium) depends on the reaction temperature, ratio of H_2/feed, hydrogen pressure – globally from the hydrotreating conditions [48], but also on resistance for sulfur (because of boron) [6,11–13] and properties of catalyst.

Therefore we can say, that two factors play main role in incomplete sulfidation of catalyst in applied conditions: (i) resistance properties of NiB alloy for poisoning by sulfur, (ii) conditions of HDS reaction influence on thermodynamic equilibrium Ni/Ni_3S_2 system.

On the basis of the XPS results obtained for amorphous boron alloy [12] it has been commonly accepted that boron gives some of its electrons to the nickel in the melt. The specific evidence leading to this conclusion was the difference in the bond energy of the elementary boron molten with nickel and pure boron [12]. Some of the boron electrons occupy the partly empty nickel orbital *d*, which makes boron electro-deficit, while nickel is electron-enriched. As a result, boron shows greater affinity to free electron pairs of e.g. sulfur or oxygen than nickel and protects the metal from sulfur

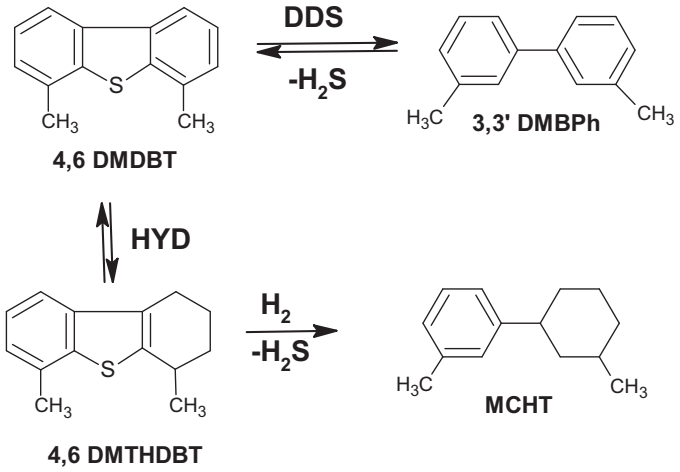

Scheme 1. Reaction pathway of the HDS of 4,6-DMDBT over bulk NiB alloy.

poisoning or oxidation. On the other hand, the electron-enriched nickel shows affinity to unsaturated bonds, so it becomes active in hydrogenation reactions [12]. Moreover, the coordination number of the Ni—Ni bond is much higher than that of the Ni—B bond. It means that the content of nickel in the Ni—B alloy is much greater than that of boron. Additionally, the atomic mass of nickel is a few times greater than that of boron, so the energy of nickel bond is not so sensitive to changes as that of the boron bond [12].

Luo et al. [11] studied theoretically the adsorption of sulfur by the density functional theory calculations. According to their results, sulfur prefers bonding to boron and not to nickel in the alloy Ni—B catalysts, which leads to protection of the active nickel from deactivation by sulfur in the catalytic reactions of hydrogenation. The results of Luo et al. [11] are fully consistent with those reported earlier by Li et al. [12] and have been confirmed by those of Wang et al. [13], who postulated that in NiB alloys sulfur is reversibly adsorbed on elementary boron.

4.2. Hydrodesulfurization

Model reaction of 4,6-DMDBT ran on the bulk NiB alloy in both variants – with and without the carbazole HDN process – takes place either via the direct desulfurization route (DDS), producing 3,3′-DMBPh, or via the hydrogenation route (HYD), producing MCTH. This is presented in the Scheme 1. Generally, course of the reaction resembles the cases of classical sulfide or metallic catalysts, e.g. Pd/Al_2O_3 [50]. For the Pd/Al_2O_3 metallic catalyst, out of the two possible routes of the reaction, HYD is the dominant one [50], which was also observed in our case (active phases Ni and Ni_3B). Due to the steric hindrance in the 4,6-DMDBT particle, which prevents direct sulfur extraction, such a particle is more reactive on the hydrogenation route [51].

None of the HDS products was the product of complete hydrogenation, i.e. 3,3′-DMBCH. This compound may be created as a result of gradual hydrogenation of 4,6-DMDBT to perhydro-4,6-DMDBT, and then be subjected to desulfurization, thus directly producing 3,3′-DMBCH. The other possibility is hydrogenation of MCHT. However, in this case it is much more difficult, as hydrogenation of the second aromatic ring is much more complicated. What is more, the MCHT molecule is not flat and thus its adsorption is more difficult [52]. In our case the amount of MCHT is clearly increasing with increased contact time. Therefore, it may be assumed that MCHT is produced directly by desulfurization of hexahydro-4,6-DMDBT.

It's well known that noble metals and also nickel are active in hydrogenation reactions [53]. But, as mentioned above, Ni is very sensitive because of strong adsorption of H_2S [44]. As mentioned before, the degree of sulfur poisoning depends upon the conditions of reaction [39], the kind of sulfur compounds used [54], the surface structure and structural properties of the catalysts [55]. In NiB alloy, the Ni 3d levels are more occupied in the alloy than in pure nickel, and the d bond position is important for hydrogenation catalysis [56]. Similarly, as postulated earlier by Okamato et al. [57], the catalytic hydrogenation activity of NiB alloy is generally higher than Raney nickel, which can be attributed to higher electron density on the nickel atom, due to electron transfer from boron to nickel. Consequently, this increases resistance to poisoning of NiB by sulfur [57]. On the other hand Diplas et al. [58] suggested that the main electronic changes occurring are due to hybridization of the Ni spd states with B sp states, which causes increase of the electron density around the Ni sites.

Because of steric hindrance of methyl groups in 4,6-DMDBT, the preferential way for adsorption is flat mode by π-electrons of thiophenic compound. In this way, strong metal–thiophenic compound bonds are formed in the η^4 mode (by C—C double bonds) and η^5 (by the delocalized π-electrons) [59].

It is a well known that nickel or cobalt sulfide supported on Al_2O_3 are hardly active during the HDS reaction. However, both Co and Ni sulfides, supported on carbon as an inert carrier (as a bulk), have higher HDS activities than MoS_2/C [60] and Ni sulfide is known to possess a moderate HDS activity [61]. Additionally, Neurock and van Santen [62] postulated, based on their theoretical study, that Ni_3S_2 cluster is relatively active in HDS reaction. H_2 adsorbs and dissociates heterolytically over Ni_3S_2 to form adsorbed sulfhydryl (SH) and hydryl (MeH) species. According to Oudar [63], sulfur chemisorbed at saturated monocrystal of nickel, causes electron transfer from Ni to S. The above favors binding of hydrogen atoms, creating acid S-H acid sites – acid centers, which are present on our catalyst after HDS and HDS/HDN reactions (TPD ammonia – 5.48 $\mu mol\,g^{-1}$). These species play an active role in HDS and in hydrogenation [64,65]. Moreover, the atomic thermodynamic calculations [46] have shown that at the conditions of HDS, very small particles of non-supported Ni_3S_2 should be present mainly as Ni_3S_3 cluster (in situ) [46,66]. Results of Aray et al. [46] describing these cluster, suggest that their Lewis acidity is much larger (and therefore they are much more reactive in HDS) than Ni_3S_2. It can be seen that increasing contact time leads to increased ratio of HYD/DDS – which means that HYD route becomes more dominant – Fig. 11A and B. On the other hand, the amount of 3,3′-DMDBT being formed is almost independent of the contact time (which can be especially seen in Fig. 11A, for $t_c \geq 0.73$ s). Based on this it can be said, that main activity (HYD route) occurs on reduced Ni – species with strong hydrogenation properties. On the other hand direct desulfurization (DDS) route of the 4,6-DMDBT HDS reaction occurs mainly on Ni sulfide clusters – sulfur vacancies (coordinately unsaturated sites – CUS). Finally, the main activity of NiB alloy is attributed of Ni and boride phases.

4.3. Kinetics

In order to study the kinetics of the reaction the concentration of the substrate is plotted as a function of the contact time. The shape of the curves suggests that, in the absence of N-compound, the kinetics of the HDS reaction follows a 1st order reaction in respect to the concentration of 4,6-DMDBT. The order of the reaction is changed in the presence of N-compounds, switching from 1st order to zero order reaction in respect to the concentration of 4,6-DMDBT. Moreover, the calculated data (according the kinetics law [67]) of 4,6-DMDBT concentration versus contact time are fitting well the experimental dates – Fig. 13.

Thus, it may be assumed that for the HDS 4,6-DMDBT reaction alone there are active surfaces unsaturated with the reactant.

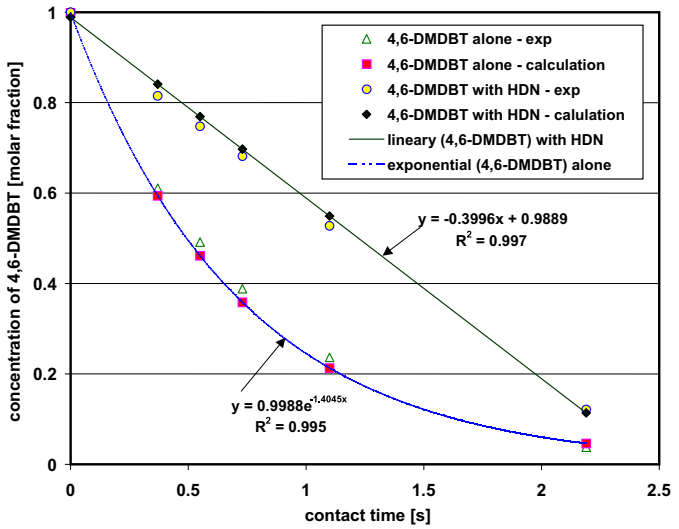

Fig. 13. Correlation between the experimental (▲, ○) and the calculated (□, ♦) data of 4,6-DMDBT concentration using the first-order rate laws formulae of global kinetics performed over a NiB alloy for alone and simultaneously reaction HDS.

Hence, the reaction depends on the substrate concentration. Yet, in the case of parallel reaction HDS/HDN, HDS reaction kinetics has changed (from first to zero order reaction). Therefore, it may be presumed that complete saturation of the catalyst active sites by reactants took place – mainly by carbazole and the remaining sites by 4,6-DMDBT. This leads to change of the HDS reaction kinetics into zero order reaction. This kinetic data suggest, that the first step of desulfurization of 4,6-DMDBT (sterically hindered S compound) and of the denitrogenation of carbazole, is hydrogenation. Both hydrogenations occur on the same active sites [68].

5. Conclusions

- Bulk NiB alloy was active in applied reaction–HDS of 4,6-DMDBT. The products of the reaction with or without N-compound were MCHT (along HYD route), main product and 3,3′-DMBPh (along DDS route) in lower amount. No fully hydrogenated products like 3,3′-dimethylbicyclohehyl (3,3′-DMBCH) were observed.
- The analysis of the obtained results suggests that, metallic Ni, Ni_3B and Ni_3S_2 were formed during the HDS reaction. The mean activity of catalyst in HDS reaction of 4,6-DMDBT can be related to presence of Ni and Ni_3B phases.
- Based on these results and calculation kinetics of reaction, it can be assumed that the rate of HDS of the 4,6-DMDBT, catalyzed by NiB alloy, is a first order reaction with respect to the substrate concentration for alone process of HDS, while for the same catalyst in case of simultaneous HDS/HDN reactions, this rate is independent of the 4,6-DMDBT concentration (zero-order) in the range of contact times studied.
- Under favorable conditions, the second stage of HDS (low H_2S partial pressure) it is possible to carry on HDS reaction on metallic phase of Ni^0 on NiB alloy catalyst.

References

[1] S.T. Wong, J.F. Lee, J.M. Chen, C.Y. Mou, J. Mol. Catal. A: Chem. 165 (2001) 159–167.
[2] R. Zhang, F. Li, N. Hang, Q. Shi, Appl. Catal. A: Gen. 239 (2003) 17–23.
[3] M. Wang, F. Li, R. Zhang, Catal. Today 93 (95) (2004) 603–606.
[4] W.-J. Wang, He-X. Li, S.-H. Xie, Y.-J. Li, J.-F. Deng, Appl. Catal. A: Gen. 184 (1999) 33–39.
[5] W.J. Wang, H. Li, Y.J. Li, J.-F. Deng, Appl. Catal. A: Gen. 203 (2000) 301–306.
[6] W.J. Wang, M.H. Qiao, H.X. Li, W.L. Dai, J.-F. Deng, Appl. Catal. A: Gen. 168 (1998) 151–157.
[7] B.-J. Liaw, S.-J. Chiang, Ch-H. Tsai, Y.-Z. Chen, Appl. Catal. A: Gen. 284 (2005) 239–246.
[8] S.-J. Chiang, Ch-H. Yang, Y.-Z. Chen, B.-J. Liaw, Appl. Catal. A: Gen. 326 (2007) 180–188.
[9] W.-J. Wang, J.-H. Shen, Y.-W. Chen, Ind. Eng. Chem. Res. 45 (2006) 8860–8865.
[10] H. Li, Q. Zhao, H. Li, J. Mol. Catal. A: Chem. 285 (2008) 29–35.
[11] C. Luo, W.N. Wang, M.H. Qiao, K.N. Fan, J. Mol. Catal. A: Chem. 184 (2002) 379–386.
[12] H. Li, H. Li, W.L. Dai, W. Wang, Z. Fang, J.-F. Deng, Appl. Surf. Sci. 152 (1999) 25–34.
[13] W.J. Wang, H.X. Li, J.-F. Deng, Appl. Catal. A: Gen. 203 (2000) 293–300.
[14] S.E. Skrabalak, K.S. Suslick, Chem. Mater. 18 (2006) 3103–3107.
[15] G.L. Parks, M.L. Pease, A.W. Burns, K.A. Layman, M.E. Bussell, X. Wang, J. Hanson, J.A. Rodriquez, J. Catal. 246 (2007) 277–292.
[16] E. Altamirano, J.A. de los Reyes, F. Murrieta, M. Vrinat, Catal. Today 133–135 (2008) 292–298.
[17] H. EP Directive 2003/EC, J. Eur. Union L76 46 (2003) 9–12.
[18] B. Alsolami, J.T. Carneiro, J.A. Moulijn, M. Makkee, Fuel 90 (2011) 3021–3027.
[19] B. Pawelec, R.M. Navarro, J.M. Campos-Martin, J.L.G. Fierro, Catal. Sci. Technol. 1 (2011) 23–42.
[20] R. Bacaud, V.L. Cebolla, L. Membrado, M. Matt, S. Pessayre, E.M. Galvez, Ind. Eng. Chem. Res. 41 (2002) 6005–6014.
[21] V. Meille, E. Schulz, Marc Lemaire, M. Vrinat, J. Catal. 170 (1997) 29–36.
[22] F. Bataille, J.-L. Lemberton, Phi. Michaud, G. Perot, M. Vrinat, M. Lemaire, E. Schulz, M. Breysse, S. Kasztelank, J. Catal. 191 (2000) 409–422.
[23] R. Prins, Adv. Catal. 46 (2001) 399–464.
[24] S. Brunauer, L.S. Deming, W.S. Deming, E. Tam, J. Am. Chem. Soc. 62 (1940) 1723–1732.
[25] K.S.W. Sing, D.H. Everet, R.A.W. Haul, L. Moscou, P.A. Pierotti, J. Rouquerol, T. Siemieniewska, Pure Appl. Chem. 57 (1985) 603–630.
[26] G. Leofanti, M. Padovan, G. Tozzola, B. Venturelli, Catal. Today 41 (1998) 207–219.
[27] J.R. Anderson, K.C. Pratt, Introduction of Characterization and Testing of Catalysts, Academic Press, New York, 1985, pp. 112.
[28] J.H. De Boer, The Structure and Properties of Porous Materials Proc X Symp. Colston Research Soc. Univ, Bristol Butterworths Sci. Publ, London, 1958, pp. 68.
[29] J.F. Deng, H. Li, W. Wang, Catal. Today 51 (1999) 113–125.
[30] H.H. Li, H.Y. Chen, S.Z. Dong, J.S. Yang, J.F. Deng, Appl. Surf. Sci. 125 (1998) 115–119.
[31] H. Li, H. Li, J.-F. Deng, Mater. Lett. 50 (2001) 41–46.
[32] H. Li, H. Li, J.-F. Deng, J. Mol. Catal. A: Chem. 169 (2001) 295–301.
[33] Z. Cheng, H. Abernathy, M. Liu, J. Phys. Chem. C. Lett. 111 (2007) 17997–18000.
[34] J.A. Schreifels, P.C. Maybury, W.E. Swartz, J. Catal. 65 (1980) 195–206.
[35] Yu.N. Bekish, T.V. Gaevskaya, L.S. Tsybulskaya, Goo-Yul Lee, M. Kim, Protection Met. Phys. Chem. Surf. 46 (2010) 325–331.
[36] M. Wang, H. Li, Y. Wu, J. Hang, Mater. Lett. 57 (2003) 2954–2964.
[37] P. Marcus, J. Oudar, I. Olefjord, Mater. Sci. Eng. 42 (1980) 191–197.
[38] H. Li, Y. Wu, Y. Wan, J. Zhang, W. Dai, M. Qiao, Catal. Today 93–95 (2004) 493–503.
[39] S. Wei, Z. Li, S. Yin, X. Zhang, W. Liu, X. Wang, J. Synchrotron Rad. 8 (2001) 566–568.
[40] J.-F. Deng, H. Li, W. Wang, Catal. Today 51 (1999) 113–125.
[41] H. Li, H. Li, J.-F. Deng, Catal. Today 74 (2002) 53–63.
[42] S. Wei, H. Oyanagi, Z. Li, X. Zhang, W. Liu, S. Yin, X. Wang, Phys. Rev. B 63 (2001) 224201(1)–224201(5).
[43] I. Bezverkhyy, G. Gadacz, J.-P. Bellat, Mater. Chem. Phys. 114 (2009) 897–901.
[44] J.R. Rostrup-Nielse, J. Catal. 21 (1971) 171–178.
[45] C.H. Bertholomew, P.K. Agrawal, J.R. Katzer, Adv. Catal. 31 (1982) 135–242.
[46] Y. Aray, A.B. Vidal, D.S. Coll, J. Rodriguez, D. Vega, J. Comput. Methods Sci. Eng. 9 (2009) 301–312.
[47] Xinjin Zhao, Theses: Nickel deposition on hydrodemetallation catalysts, Massachusetts Institute of Technology, February, 1993, pp. 35.
[48] Y. Yoshimura, M. Toba, T. Matsui, M. Harada, Y. Ichihashi, K.K. Bando, H. Yasuda, H. Ishihara, Y. Morita, T. Kameoka, Appl. Catal. A: Gen. 322 (2007) 152–171.
[49] A. Stoklosa, J. Stringert, Oxidation of Metals 11 (1977) 277–288.
[50] R. Prins, M. Egorowa, A. Röthlisberger, Y. Zhao, N. Sivasankar, P. Kukula, Catal. Today 111 (2006) 84–93.
[51] D.D. Whitehurst, I. Isoda, I. Mochida, Adv. Catal. 42 (1998) 345–471.
[52] M. Egorowa, R. Prins, J. Catal. 224 (2004) 278–287.
[53] V.L. Barrio, P.L. Arias, J.F. Cambra, M.B. Guemez, B. Pawelec, J.L.G. Fierro, Appl. Catal. A: Gen. 242 (2003) 17–30.
[54] J. Barbier, E. Lamy-Pitara, P. Marecot, J.P. Boitiaux, J. Cosyns, F. Verna, Adv. Catal. 37 (1990) 279–318.
[55] V.L. Barrio, P.L. Arias, J.F. Cambra, M.B. Guemez, J.M. Campos-Martin, B. Pawelec, J.L.G. Fierro, Appl. Catal. A: Gen. 248 (2003) 211–225.
[56] S. Diplas, O.M. Lovvik, J. Phys.: Condens. Matter 21 (2009) 245503(1)–245503(9).
[57] Y. Okamoto, Y. Nitta, T. Imanaka, S. Teramishi, J. Catal. 64 (1980) 397–404.
[58] S. Diplas, J. Lehrmann, S. Jorgensen, T. Valand, J.F. Watts, J. Tafto, Surf. Inter. Anal. 37 (2005) 459–465.
[59] D.R. Huntley, D.R. Mullins, M.P. Wingeier, J. Phys. Chem. 100 (1996) 19620–19627.
[60] J.C. Duchen, E.M. van Oess, V.H.J. de Beer, R. Prins, J. Catal. 80 (1983) 386–402.
[61] P. Afanasiev, I. Bezverkhyy, Appl. Catal. A: Gen. 322 (2007) 129–141.

[62] M. Neurock, R.A. van Santen, J. Am. Chem. Soc. 116 (1994) 4427–4439.
[63] J. Oudar, Catal. Rev. Sci. Eng. 22 (1980) 171–195.
[64] N. Topsoe, H. Topsoe, J. Catal. 139 (1993) 641–651.
[65] A. Olivas, J. Cruz-Reyes, V. Petranovskii, M. Alvalos, S. Fuentes, J. Vac. Sci. Technol. A 16 (1998) 3515–3520.
[66] M. Yamada, H. Hirashima, A. Kitada, K. Izumi, J. Nakamura, Surf. Sci. 602 (2008) 1659–1668.
[67] M. Boudart, G. Djéga-Mariadassou, Kinetics of Heterogeneous Catalytic Reactions, Princeton University Press, Princeton, 1984.
[68] P. Zeuthen, K.G. Knutsen, D.D. Whitchurst, Catal. Today 65 (2001) 307–314.